

Discrete spherical means of directional derivatives and their applications

Alexander Belyaev^{*} Boris Khesin[†] Serge Tabachnikov[‡]

Abstract

The goal of this paper is two-fold. First we study theoretical properties of discrete spherical means of directional derivatives of a function. Then we focus on the two-dimensional case and use discrete circular means to derive rotation-equivariant discrete approximations of linear and nonlinear first- and second-order differential operators. Applications to nonlinear filtering of digital images and surface curvature estimation are considered.

Introduction

Mean value properties of functions play crucial role in analysis of many partial differential equations [8], numerical interpolation and integration [25], computer tomography [17], and many other areas of mathematics and engineering. In this paper we undertake a study of discrete spherical means of directional derivatives of functions. We analyze general properties of such means (Section 1), and use them to derive rotation-equivariant discrete approximations of linear and nonlinear first- and second-order differential operators (Section 2). The two principal components of our approach are based on the use of the Veronese maps [10] and Minkowski's existence theorem [23]. Possible applications of the described discretizations include, in particular, the Laplace-Beltrami operator on manifolds. The Laplacian case is particularly useful in computations related to the fast dynamo problem, where the

^{*}Heriot-Watt University, Edinburgh, UK

[†]Department of Mathematics, University of Toronto, Canada

[‡]Department of Mathematics, Pennsylvania State University, USA

proposed formulas may simplify computations of the magnetic diffusion for iterations of a seed magnetic field, see [6].

1 Discrete spherical means of derivatives

General construction and Veronese maps. Consider the following general

Problem. *Given a degree $k \neq 0$ and a collection of points $P_i, i = 1, \dots, N$ in general position on the unit sphere in $S^n \subset \mathbf{R}^{n+1}$, find weights w_i such that for every spherical harmonic F of the degree k one has $\sum_i w_i \cdot F(P_i) = 0$.*

Note that for a possible application to computations of the mean curvature of a manifold, the function F can be the sum of a constant ($k = 0$) and a homogeneous quadratic term ($k = 2$), and one needs to find the weights for obtaining the mean value \bar{F} of such a function from its values at the given set of points. (Of course, all nonzero harmonics should give us the zero mean.) The cases of computations for the discrete Laplacian and square gradient operators are similar.

Remark. This problem is very close to constructions of so called “spherical designs.” The latter is a finite set of points on S^n such that the average value of any polynomial F of degree less than or equal to k on this set equals the average value of the polynomial F on the sphere. The concept of a spherical design was introduced in [7]. The existence and structure of spherical designs in a circle was studied in [11]. In [24] the existence of designs of all sufficiently large sizes was proved: there is a number $N(n, k)$ depending on n and k , such that a design exists for any $N > N(n, k)$. Many examples and recent results can be found in the survey [2].

The problem posed above is somewhat different: we do not require the weights to be equal. In many applications, however, one uses the regular lattices, and the weights turn out to be equal, as we discuss below. On the other hand, the problem under discussion is also related to the following Minkowski theorem: the sum of the outward normal vectors to the faces of a convex polyhedron is zero, provided the magnitudes of these vectors equal the areas of the respective faces. The Minkowski problem asks whether the converse is true: given unit vectors P_i in \mathbf{R}^{n+1} and positive weights w_i such that $\sum w_i \cdot P_i = 0$, find a convex polyhedron whose faces are orthogonal

to the directions P_i and the weights are the n -dimensional volumes of the corresponding faces. The Minkowski problem has a unique solution if the vectors P_i span \mathbf{R}^{n+1} .

Construction. First, we solve the above Problem for a linear functional L (i.e. for $k = 1$). In this case the solution is given by the Minkowski theorem. Namely, consider the tangent hyperplanes to the sphere S^n at points P_i ; they form a polyhedron. (Here it suffices to assume that $P_i, i = 1, \dots, N$ are in general position, i.e., not lying at one hyperplane section of the sphere.) Let w_i be the signed codimension-one volumes of the faces of this polyhedron. Then $\sum_i w_i \cdot P_i = 0$ according to the Minkowski theorem (where we understand P_i as vectors in \mathbf{R}^{n+1}), and hence $\sum_i w_i \cdot L(P_i) = 0$ for every linear function.

Next, consider harmonic polynomials of degree k in \mathbf{R}^{n+1} restricted to the sphere $S^n \subset \mathbf{R}^{n+1}$. We take harmonic ones since they give exactly all independent restrictions of homogeneous polynomials of degree k from \mathbf{R}^{n+1} to the sphere. (We will need the restrictions of x_1^2, \dots, x_{n+1}^2 for the curvature function.)

Now we consider the harmonic Veronese map $V : \mathbf{R}^{n+1} \rightarrow \mathbf{R}^q$, where $V(x_1, \dots, x_{n+1}) = (x_1^k - x_2^k, \dots)$ (a basis of harmonic polynomials in x_1, \dots, x_{n+1} of degree k). The dimension q is given by the formula: $q = \binom{n+k-1}{n-1} - \binom{n+k-3}{n-1}$. Then $F = L \circ V$ where L is a linear function on \mathbf{R}^q . Let w_j be the constructed above weights for the collection of points $V(P_j)$ in \mathbf{R}^q . This gives us the required formula $\sum_i w_i \cdot F(P_i) = 0$.

Example 1. Let us demonstrate this approach in the case of a circle S^1 and quadratic functions. The harmonic Veronese map for quadratic polynomials sends the coordinate functions $\{x_1, \dots, x_{n+1}\}$ to the space of quadratic harmonic polynomials (whose restrictions on the sphere S^n give us spherical harmonics). For the circle $S^1 \subset \mathbf{R}^2$ this harmonic Veronese map is $V : \mathbf{R}^2 \rightarrow \mathbf{R}^2$, where $(x, y) \mapsto (x^2 - y^2, 2xy)$, or $(\cos \phi, \sin \phi) \mapsto (\cos 2\phi, \sin 2\phi)$, see a detailed analysis in the next section.

Note that if we map $\mathbf{R}_{x,y}^2$ to the full 3-dimensional space \mathbf{R}^3 of quadratic polynomials $(x^2, y^2, 2xy)$, then the image of the circle $S^1 \subset \mathbf{R}^2$ will lie in the plane $\mathbf{R}^2 \subset \mathbf{R}^3$ (due to the relation $x^2 + y^2 = 1$), so the point images $V(P_i)$ will not be in general position to yield a polyhedron circumscribed around a 2-sphere in \mathbf{R}^3 .

Example 2. For the case of 2-sphere and quadratic functions the space of harmonic polynomials is 5-dimensional, and our harmonic Veronese map sends S^2 to this \mathbf{R}^5 . The point images lie in general position, and sufficiently many points (at least 6) would yield a polyhedron, which allows one to find the corresponding weights w_i .

Remark. Since the points $Q_j = V(P_j)$ should lie on the sphere S^{q-1} , rather than be generic vectors in \mathbf{R}^q , one can project them to the sphere by rescaling. Namely, let Q_j be a (sufficiently generic) collection of non-zero vectors in \mathbf{R}^q . Assign the following weights w_j to these vectors. Consider the collection of points $Q_j/|Q_j|$ on the unit sphere S^{q-1} , draw the tangent hyperplanes to the sphere, and let u_j be the signed $(q-1)$ -dimensional volumes of the faces of the resulting polyhedron.

Proposition. For every linear function L on \mathbf{R}^q , one has: $\sum_j w_j \cdot L(Q_j) = 0$, where the weights are $w_j := u_j/|Q_j|$.

PROOF. The Minkowski formula says that $\sum u_j \cdot Q_j/|Q_j| = 0$, hence $0 = \sum u_j \cdot L(Q_j)/|Q_j| = \sum_j w_j \cdot L(Q_j)$. QED

Weights for regular lattices. Now, from the general consideration of points in general position we move to regular ones, and consider the set of all “ m -mid-points,” i.e., the set $M_m \subset S^n$ of points whose coordinates are all possible combinations of m nonzero coordinates equal to ± 1 among n spots, starting with $(\pm 1, \dots, \pm 1, 0, \dots, 0)$ to $(0, \dots, 0, \pm 1, \dots, \pm 1)$, which are scaled to belong to the unit sphere $S^n \subset \mathbf{R}^{n+1}$.

Example 3. In dimension 3, for $m = 1$ we get M_1 consisting of 6 midpoints of the cube faces, which are also the vertices of an octahedron: $(\pm 1, 0, 0)$, $(0, \pm 1, 0)$ and $(0, 0, \pm 1)$. The set M_2 consists of 12 scaled mid-points of the cube edges: $(\pm 1, \pm 1, 0)/\sqrt{2}$, $(\pm 1, 0, \pm 1)/\sqrt{2}$, and $(0, \pm 1, \pm 1)/\sqrt{2}$. The set M_3 contains exactly 8 vertices of the cube: $(\pm 1, \pm 1, \pm 1)/\sqrt{3}$.

Theorem. Let $F(x_1, \dots, x_{n+1})$ be a homogeneous quadratic function, $M_m \subset S^n$ be the set of m -mid-points. Then

$$\frac{1}{\text{vol}(S^n)} \int_{S^n} F \, dS = \frac{1}{\#M_m} \sum_{x \in M_m} F(x),$$

where $\text{vol}(S^n)$ is the volume of n -dimensional sphere and $\#M_m$ is the number of points in M_m .

One can see that in all these “regular cases” one counts the points of M_m with equal weights. This theorem generalizes the corresponding 3D consideration (see e.g. [18]), which gives three basis stencils used in the Laplacian computations.

PROOF. Write $F = c + G$, where $c \in \mathbf{R}$ and G a harmonic quadratic polynomial. For a constant c the claim is obvious. For G one has $\int_{S^n} G dS = 0$, so we need to show that $\sum_{x \in M_m} G(x) = 0$ for every harmonic quadratic polynomial G .

Consider the full Veronese map $\bar{V} : \mathbf{R}^n \rightarrow \mathbf{R}^{q+1}$, given by

$$(x_1, \dots, x_{n+1}) \mapsto (x_1^2, \dots, x_{n+1}^2; x_1x_2, \dots, x_nx_{n+1}),$$

with $q + 1 = (n + 1)(n + 2)/2$. Let \mathcal{H} be the space of linear functions on \mathbf{R}^{q+1} that vanish on the vector $\xi = (1, \dots, 1; 0, \dots, 0)$ with first $n + 1$ nonzero components (we separate them by semicolon). Then, for each quadratic harmonic G , one has $G = H \circ \bar{V}$ for some $H \in \mathcal{H}$. Indeed, harmonic polynomials form a hyperplane in the space of linear functions on \mathbf{R}^{q+1} being given by one linear relation (coming from the sphere equation $x_1^2 + \dots + x_{n+1}^2 = 1$), and the polynomials $x_1^2 - x_2^2, \dots, x_n^2 - x_{n+1}^2, x_1x_2, \dots, x_nx_{n+1}$ are harmonic and equal to 0 on this vector ξ . Thus we need to check that $\sum_{Q \in \bar{V}(M_m)} H(Q) = 0$ for all $H \in \mathcal{H}$ and any $m = 1, \dots, n + 1$.

For instance, for the set M_1 , which consists of $(0, \dots, 0, \pm 1, 0, \dots, 0)$ -type points, the image $\bar{V}(M_1)$ consists of vectors Q_i : $(0, \dots, 0, 1, 0, \dots, 0; 0, \dots, 0)$ with 1's in one of the first n coordinates. In the case of M_2 with $2n(n - 1)$ “diagonal” points $(0, \dots, 0, \pm 1, 0, \dots, 0, \pm 1, 0, \dots, 0)/\sqrt{2}$, the image $\bar{V}(M)$ consists of vectors Q_i :

$$(0, \dots, 0, 1, 0, \dots, 0, 1, 0, \dots, 0; 0, \dots, 0, \pm 1, 0, \dots, 0)/2$$

with all possible pairs of 1's among first $n + 1$ coordinates and the ± 1 at the respective, ij -place. Similarly, for any m one can see that in each of these cases we have $\sum_1^{\#M_m} Q_i = \text{const} \cdot \xi$. Hence $\sum_1^{\#M_m} H(Q_i) = 0$ for all $H \in \mathcal{H}$, as claimed. QED.

Remark. For computations we are often interested mostly in the case $S^2 \subset \mathbf{R}^3$. Here is the explicit statement for $M = M_2$ adjusted to this case: let $F(x, y, z)$ be a homogeneous quadratic function, $M \subset S^2$ be the set of 12 points: $(\pm 1, \pm 1, 0)/\sqrt{2}, (\pm 1, 0, \pm 1)/\sqrt{2}, (0, \pm 1, \pm 1)/\sqrt{2}$. Then

$$\frac{1}{4\pi} \int_{S^2} F dS = \frac{1}{12} \sum_{P \in M} F(P).$$

Thus in all of the above cases we need to use the same weights on these points. This equality of weights for a given set M_m can also be obtained from the symmetry consideration. One can also take combination of the above lattices M_m with *any weights* (provided that the sum of the weights is equal to 1): e.g., by considering arbitrary combinations of the 3 lattices in \mathbf{R}^3 : mid-edges, vertices of the cube, and at the middle of faces. By imposing additional requirements, one can optimize these coefficients: for instance, to achieve an isotropic approximation, or with the next approximation smallest in an appropriate sense.

Remark. Points of $\overline{V}(M_1)$, evidently, form the coordinate $(n + 1)$ -simplex in the space spanned by first $n + 1$ coordinates, which is a slim subspace in \mathbf{R}^{q+1} . In the case of M_2 , the points of $\overline{V}(M_2)$ form the standard q -simplex in a hyperplane in \mathbf{R}^{q+1} . Indeed, in the latter case, we see that for all $Q_i \in \overline{V}(M_2)$ one has $(Q_i, Q_j) = 1/2$ for $i \neq j$ and $(Q_i, Q_i) = 3/4$, i.e., the vectors Q_i have the same length and same angles between them.

Remark. Above we considered two discretization procedures, both using the Veronese map: a generic set of points $\{P_i\}$ and the mid-points sets. While for a generic set in \mathbf{R}^{q+1} the coefficients are given by the Minkowski formula for the corresponding polyhedron in the image, it is not the case in the mid-point cases. Indeed, due to a very regular structure of the image points $Q_j = \overline{V}(P_j)$, the corresponding tangent planes go to infinity, and the corresponding volumes of the faces are infinite.

In a sense, if the image points Q_j are linearly dependent in $\mathbf{R}^{q+1}(\text{ mod } \xi)$, and the corresponding polyhedron has faces going to infinity (like in the standard basis case), we have to quotient out these “directions to infinity,” and consider the volume of faces in a polyhedron of smaller dimension.

Example 4. For $n = 2$ and for the standard basis we did not get a polygon on the plane $\mathbf{R}^2 = \mathbf{R}^3(\text{ mod } \xi)$. Instead, it reduces to a pair of points in \mathbf{R}^1 . It is not enough to start with two generic points in this case, but if we take three generic points on the circle, we obtain an interpolation formula. This is a manifestation of the general phenomenon described in the following proposition.

Proposition. *There is no discrete mean value formula for quadratic harmonics and a given generic collection of $n + 1$ points on S^n .*

PROOF. Let $P_1, \dots, P_{n+1} \in S^n$, and let $\bar{V} : \mathbf{R}^{n+1} \rightarrow \mathbf{R}^{q+1}$ with $q + 1 = (n + 1)(n + 2)/2$ be the full Veronese map:

$$(x_1, \dots, x_n) \mapsto (x_1^2, \dots, x_{n+1}^2; x_1x_2, \dots, x_ix_j, \dots).$$

Let $\bar{V}(P_k) = Q_k$. Let $\xi = (1, \dots, 1; 0, \dots, 0) \in \mathbf{R}^{q+1}$.

We want to find constants w_k such that $\sum w_k \cdot Q_k = \xi$. This is equivalent to the following equality:

$$Diag(w_k) = (A^*A)^{-1},$$

where A is the matrix made of the vectors P_1, \dots, P_{n+1} , as the following linear algebra shows. Indeed, the equality $\sum w_k Q_k = \xi$ is equivalent to

$$\sum_i w_i x_{k,i} x_{l,i} = \delta_{k,l},$$

which is equivalent to $A \cdot Diag(w) \cdot A^* = E$, the identity matrix. This is equivalent to $(A^*A)^{-1} = Diag(w)$, as claimed.

Of course, if $\{P_k\}$ is an orthonormal frame then A is orthogonal, and all $w_k = 1$, as in the Theorem above. The matrix AA^* is diagonal if and only if the vectors P_i are pairwise orthogonal. This is the case for the set M_1 discussed above, which consists of the basis points, but, of course, not true for generic collection of $n + 1$ points on S^n . This implies that one cannot have an interpolation formula with $n + 1$ generic points. QED

Note that on the other hand, if one has sufficiently many points, so that their Veronese images are linearly dependent in $\mathbf{R}^{n(n+1)/2} \pmod{\xi}$, then any such linear relation provides the weights that yield an interpolation formula.

2 Circular means of derivatives

A simple way to demonstrate rotational invariance of the Laplacian

$$\Delta \equiv \frac{\partial^2}{dx^2} + \frac{\partial^2}{dy^2}$$

consists of representing it as the circular mean (the spherical mean in 3D) of the second-order directional derivatives

$$\frac{1}{2}\Delta f = \frac{1}{\pi} \int_0^\pi \frac{\partial^2 f}{\partial e_\varphi^2} d\varphi, \quad \text{where} \quad \frac{\partial}{\partial e_\varphi} = \cos \varphi \frac{\partial}{\partial x} + \sin \varphi \frac{\partial}{\partial y}. \quad (1)$$

The rotational invariance of squared gradient $|\nabla f|^2$ can be demonstrated in a similar way

$$\frac{1}{2}|\nabla f|^2 = \frac{1}{\pi} \int_0^\pi \left(\frac{\partial f}{\partial e_\varphi} \right)^2 d\varphi. \quad (2)$$

A similar mean value representation for a directional derivative of f can be obtained from

$$\frac{1}{2} \left[a \frac{\partial f}{\partial x} + b \frac{\partial f}{\partial y} \right] = \frac{1}{\pi} \int_0^\pi [a \cos \varphi + b \sin \varphi] \frac{\partial f}{\partial e_\varphi} d\varphi \quad (3)$$

where a and b are constants. Notice that (3) with $a = \partial/\partial x$ and $b = \partial/\partial y$ implies (1) and setting $a = \partial f/\partial x$ and $b = \partial f/\partial y$ yields the equality (2).

Let us now derive discrete counterparts of the above mean value representations (1), (2), and (3). Consider a set of directions $e_k = (\cos \varphi_k, \sin \varphi_k)$, $k = 1, 2, \dots, n$. Then a weighted sum of second-order directional derivatives can be expressed as

$$\begin{aligned} \sum w_k \frac{\partial^2 f}{\partial e_{\varphi_k}^2} &= \frac{\partial^2 f}{\partial x^2} \sum w_k \cos^2 \varphi_k + \frac{\partial^2 f}{\partial y^2} \sum w_k \sin^2 \varphi_k \\ &+ 2 \frac{\partial^2 f}{\partial x \partial y} \sum w_k \cos \varphi_k \sin \varphi_k = \frac{1}{2} \Delta f \sum w_k \\ &+ \frac{1}{2} \left(\frac{\partial^2 f}{\partial x^2} - \frac{\partial^2 f}{\partial y^2} \right) \operatorname{Re} \left(\sum w_k e^{2i\varphi_k} \right) + \frac{\partial^2 f}{\partial x \partial y} \operatorname{Im} \left(\sum w_k e^{2i\varphi_k} \right). \end{aligned} \quad (4)$$

Finding weights $\{w_k\}$ such that

$$\sum w_k e^{2i\varphi_k} = 0 \quad (5)$$

yields, after a simple normalization

$$\{w_k\} \longrightarrow \left\{ w_k / \sum w_k \right\},$$

a discrete mean value representation for Δf

$$\frac{1}{2} \Delta f = \sum w_k \frac{\partial^2 f}{\partial e_{\varphi_k}^2}, \quad (6)$$

and similar representations of the squared gradient

$$\frac{1}{2} |\nabla f|^2 = \sum w_k \left(\frac{\partial f}{\partial e_{\varphi_k}} \right)^2 \quad (7)$$

and directional derivative

$$\frac{1}{2} \left[a \frac{\partial f}{\partial x} + b \frac{\partial f}{\partial y} \right] = \sum w_k [a \cos \varphi_k + b \sin \varphi_k] \frac{\partial f}{\partial e_{\varphi_k}}, \quad (8)$$

respectively. Obviously the same set of weights $\{w_k\}$ can be used to obtain a discrete mean value representation for a quasi-Laplacian

$$\frac{1}{2} \nabla \cdot (a(x, y) \nabla f) = \sum w_k \frac{\partial}{\partial e_{\varphi_k}} \left(a(x, y) \frac{\partial f}{\partial e_{\varphi_k}} \right). \quad (9)$$

Note that the appearance of double angles in the formula (5) exactly corresponds to the Veronese map $V : (\cos \phi, \sin \phi) \mapsto (\cos 2\phi, \sin 2\phi)$, considered in Example 1 of the preceding Section.

Discrete mean value formulas and Minkowski problem for polygons.

Note that in (1), (2), and (3) we deal with the directions $e(\varphi) = (\cos \varphi, \sin \varphi)$, $0 \leq \varphi < \pi$, which can be parameterized by the unit vector $e^{2i\varphi}$.

The geometric meaning of (5) is simple. Consider a closed polygon such that the vectors $e^{2i\varphi_k}$ are the outward normals of the polygon's edges. Then, according to the Gauss divergence theorem, the edge lengths provide us with the desired set of weights $\{w_k\}$. Vice versa, given a set of unit vectors $\{e^{2i\varphi_k}\}$ and positive weights $\{w_k\}$ satisfying the first condition in (5), the Minkowski Problem (sometimes it is called Minkowski's existence theorem, see e.g. [23]), guarantees an existence of a convex polygon with edge lengths $\{w_k\}$ and outward normals $e^{2i\varphi_k}$. The left image of Figure 1 illustrates this geometric interpretation of (5).

In particular, if we consider a polygon circumscribed around the unit circle, as seen in the middle image of Figure 1, the weights are given by

$$w_j = \frac{\tan \beta_{j-1} + \tan \beta_j}{\sum (\tan \beta_{k-1} + \tan \beta_k)}, \quad \beta_k = \varphi_{k+1} - \varphi_k. \quad (10)$$

This set of weights was used in [15] for estimating the mean curvature on surfaces approximated by dense triangle meshes.

Rotation-equivariant stencils for gradient and Laplacian.

Consider a two-dimensional square grid with step-size $h \ll 1$. Each grid vertex has eight nearest neighbors: two horizontal, two vertical, and four diagonal.

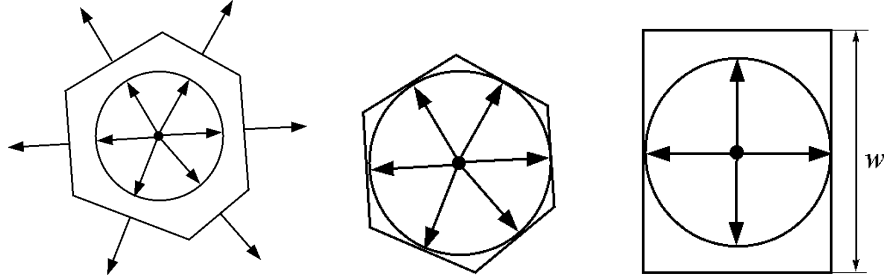


Figure 1: Left: Minkowski's existence theorem for polygons provides us with a geometric interpretation of (5). Middle: a special case of a polygon circumscribed around the unit circle was considered in [15] in connection with the curvature estimation approach proposed there. Right: 3×3 stencils for estimating the gradient and Laplacian of functions defined on a square grid contain four directions and correspond to rectangles.

Thus, according to our geometric interpretation of (6), (7), and (8), we are given four directions $\varphi = 0, \pi/4, \pi/2, 3\pi/4$, which define four unit normals

$$\{e^{2i\varphi}\}, \quad \varphi = 0, \pi/4, \pi/2, 3\pi/4,$$

and, therefore, correspond to a rectangle aligned with the coordinate axes.

Consider such a rectangle with the edge lengths 2 and w , as shown in the right image of Figure 1), and replace the first- and second-order directional derivatives in (6), (7), and (8) by corresponding central differences. We arrive at the following stencils for the x -derivative and Laplacian

$$\frac{1}{2h(w+2)} \begin{bmatrix} -1 & 0 & 1 \\ -w & 0 & w \\ -1 & 0 & 1 \end{bmatrix} \quad (11)$$

and

$$\frac{1}{h^2(w+2)} \begin{bmatrix} 1 & w & 1 \\ w & -4(w+1) & w \\ 1 & w & 1 \end{bmatrix}, \quad (12)$$

respectively. The stencil for $\partial/\partial y$ is obtained from (11) by $\pi/2$ -rotation. Here and everywhere below the 3×3 matrices are understood as finite difference operators acting on functions defined on a square grid with step-size h .

The standard central difference and five-point Laplacian is obtained when $w = \infty$. Setting $w = 1$ leads to the so-called Prewitt masks for the 1st-order

derivatives and Laplacian [22, 9]. The case $w = 2$ is commonly used in image processing applications and yields the standard Sobel mask for the derivative [22, 9] and a 9-point discrete Laplacian, which possesses good isotropic properties [12]. The case $w = 4$ was analyzed in [3], where it was shown that

$$\frac{1}{8h} \begin{bmatrix} -1 & 0 & 1 \\ -4 & 0 & 4 \\ -1 & 0 & 1 \end{bmatrix} = \frac{\partial}{\partial x} + \frac{h^2}{12} \Delta \frac{\partial}{\partial x} + O(h^4), \quad (13)$$

$$\frac{1}{6h^2} \begin{bmatrix} 1 & 4 & 1 \\ 4 & -20 & 4 \\ 1 & 4 & 1 \end{bmatrix} = \Delta + \frac{h^2}{12} \Delta^2 + O(h^4), \quad (14)$$

as $h \rightarrow 0$. Since the Laplacian is isotropic, the right hand sides of (13) and (14) deliver optimal rotation-equivariant 3×3 stencils for the x -derivative and Laplacian, respectively, for $h \ll 1$. In particular, this explains why (12) with $w = 4$ is often used for a numerical solution of the Poisson equation [13, Chapter 3, §1], [4, Chapter 3, §10].

Discrete nine-point Laplacian (12) can be represented as a linear combination of two basis five-point Laplacians

$$L_w \equiv \frac{1}{h^2(w+2)} \begin{bmatrix} 1 & w & 1 \\ w & -4(w+1) & w \\ 1 & w & 1 \end{bmatrix} = \alpha L_+ + \beta L_\times$$

with

$$\alpha = \frac{w}{w+2} \quad \text{and} \quad \beta = \frac{2}{w+2},$$

where

$$L_+ = \frac{1}{h^2} \begin{bmatrix} 0 & 1 & 0 \\ 1 & -4 & 1 \\ 0 & 1 & 0 \end{bmatrix} \quad \text{and} \quad L_\times = \frac{1}{2h^2} \begin{bmatrix} 1 & 0 & 1 \\ 0 & -4 & 0 \\ 1 & 0 & 1 \end{bmatrix}.$$

Setting $w = 4$ yields $\alpha = 2/3$ and $\beta = 1/3$.

In Figure 2, we use a Gaussian bump function

$$g(x, y) = \exp(-x^2 - y^2) \quad (15)$$

to test isotropic properties of four discrete stencils $L_\infty \equiv L_+$, $L_0 \equiv L_\times$, L_2 , and L_4 . Namely, the figure displays contour lines of $(\Delta - L_w)[g]$. As (14) suggests, L_w with $w = 4$ demonstrates the best performance.

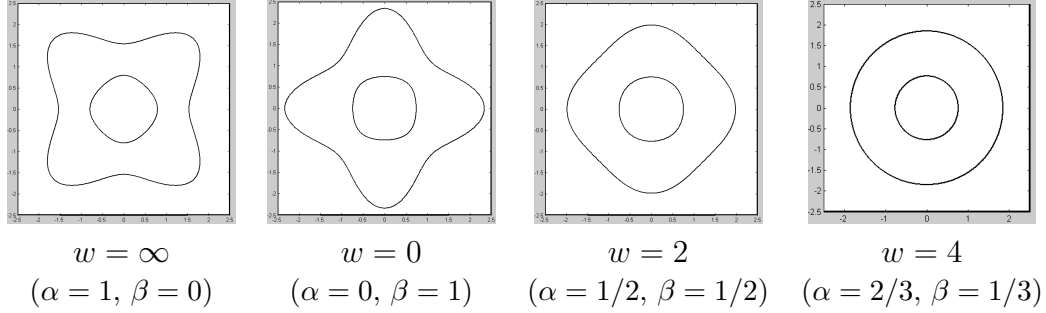


Figure 2: Contour lines of $(\Delta - L_w)[g]$ for various values of w . The best performance is achieved for $w = 4$.

Similar results are obtained for the x -derivative 3×3 stencils (11) and corresponding y -derivative stencil. Analogously to the case of the Laplacian, expansion (13) implies that (11) with $w = 4$ is rotationally optimal.

Rotation-equivariant stencil for quasi-Laplacian. Consider now a quasi-Laplacian operator

$$L^a \equiv \nabla \cdot [a(x, y)\nabla] = a\Delta + \nabla a \cdot \nabla \quad (16)$$

where $a(x, y)$ is given. In view of (14), (13), and (9), the optimal 3×3 stencils for L^a are obtained from (12) and (11) when $w = 4$.

In practice, the diffusion coefficient $a(x, y)$ in (16) is defined at the staggered grid points which lie on halfway between the standard grid points. Following [1, A.3.2] let us approximate (16) using a linear combination of two basis stencils

$$\alpha L_+^a + \beta L_\times^a$$

with

$$L_+^a[f] \equiv \frac{1}{h^2} \left[a_{+0} f_{i+1,j} + a_{-0} f_{i-1,j} + a_{0+} f_{i,j+1} + a_{0-} f_{i,j-1} - (a_{+0} + a_{-0} + a_{0+} + a_{0-}) f_{i,j} \right]$$

and

$$L_\times^a[f] \equiv \frac{1}{2h^2} \left[a_{++} f_{i+1,j+1} + a_{--} f_{i-1,j-1} + a_{+-} f_{i+1,j-1} + a_{-+} f_{i-1,j+1} - (a_{++} + a_{--} + a_{+-} + a_{-+}) f_{i,j} \right],$$

where $a_{\pm 0}$, $a_{0\pm}$, and $a_{\pm\pm}$ denote the values of $a(x, y)$ at $((i \pm 1/2)h, jh)$, $(ih, (j \pm 1/2)h)$, and $((i \pm 1/2)h, (j \pm 1/2)h)$, respectively.

Assume $h \ll 1$. Since the same weights are used in the discrete directional mean value representations (6) and (9) we can expect that the optimal rotation-equivariant stencil for quasi-Laplacian L^a is obtained when $\alpha = 2/3$ and $\beta = 1/3$, or equivalently, when $w = 4$. Indeed, straightforward calculations show that

$$\begin{aligned} L^a[f] &= \nabla \cdot [a(x, y)\nabla f] \\ &+ \frac{h^2}{12} \left[D_{0,4}(a, f) + 2D_{1,3}(a, f) + \frac{3}{2}D_{2,2}(a, f) + \frac{1}{2}D_{3,1}(a, f) \right] + O(h^4) \end{aligned} \quad (17)$$

with

$$\begin{aligned} D_{0,4}(a, f) &= a(x, y) \left(\frac{\partial^4 f}{\partial x^4} + 2\frac{\partial^4 f}{\partial x^2 \partial y^2} + \frac{\partial^4 f}{\partial y^4} \right), \\ D_{1,3}(a, f) &= \frac{\partial a}{\partial x} \frac{\partial^3 f}{\partial x^3} + \frac{\partial a}{\partial y} \frac{\partial^3 f}{\partial x^2 \partial y} + \frac{\partial a}{\partial x} \frac{\partial^3 f}{\partial x \partial y^2} + \frac{\partial a}{\partial y} \frac{\partial^3 f}{\partial y^3}, \\ D_{2,2}(a, f) &= \frac{\partial^2 a}{\partial x^2} \frac{\partial^2 f}{\partial x^2} + \frac{\partial^2 a}{\partial y^2} \frac{\partial^2 f}{\partial y^2} + \frac{4}{3} \frac{\partial^2 a}{\partial x \partial y} \frac{\partial^2 f}{\partial x \partial y} + \frac{1}{3} \frac{\partial^2 a}{\partial x^2} \frac{\partial^2 f}{\partial y^2} + \frac{1}{3} \frac{\partial^2 a}{\partial y^2} \frac{\partial^2 f}{\partial x^2}, \\ D_{3,1}(a, f) &= \frac{\partial^3 a}{\partial x^3} \frac{\partial f}{\partial x} + \frac{\partial^3 f}{\partial x^2 \partial y} \frac{\partial f}{\partial y} + \frac{\partial^3 f}{\partial x \partial y^2} \frac{\partial f}{\partial x} + \frac{\partial^3 a}{\partial y^3} \frac{\partial f}{\partial y}. \end{aligned}$$

Let us now demonstrate that these differential quantities are rotationally invariant. Obviously $D_{0,4}(a, f)$ equals $a(x, y)\Delta^2 f$ which is rotationally invariant. Let us consider

$$R_{1,3}(a, f, \varphi) = \frac{\partial a}{\partial e_\varphi} \cdot \frac{\partial^3 f}{\partial e_\varphi^3}, \quad R_{2,2}(a, f, \varphi) = \frac{\partial^2 a}{\partial e_\varphi^2} \cdot \frac{\partial^2 f}{\partial e_\varphi^2}, \quad R_{3,1}(a, f, \varphi) = \frac{\partial^3 a}{\partial e_\varphi^3} \cdot \frac{\partial f}{\partial e_\varphi}.$$

Note that $R_{3,1}(a, f, \varphi) = R_{1,3}(f, a, \varphi)$ and $D_{1,3}(a, f) = D_{3,1}(a, f)$. Direct calculations show that

$$\int_0^{2\pi} R_{1,3}(a, f, \varphi) d\varphi = \frac{3\pi}{4} D_{1,3}(a, f) \quad \text{and} \quad \int_0^{2\pi} R_{2,2}(a, f, \varphi) d\varphi = \frac{3\pi}{4} D_{2,2}(a, f).$$

This completes our proof that the $O(h^2)$ term in (17) is rotation invariant.

Application to nonlinear diffusion image filtering. Accurate numerical implementations of nonlinear diffusion processes governed by

$$\frac{\partial u(x, y, t)}{\partial t} = \operatorname{div} (a(x, y, u, \nabla u) \nabla u), \quad u(x, y, 0) = u_0(x, y), \quad (18)$$

subject to appropriate boundary conditions, are important for a number of disciplines including computational physics, magnetohydrodynamics, financial mathematics, and image processing. In particular, in image processing, adaptive image smoothing is often carried out by (18) with

$$a(x, y, u, \nabla u) = \exp(-|\nabla u|/\lambda), \quad (19)$$

as suggested by Perona and Malik in their seminal paper [19]. Figure 3 demonstrates how our numerical implementation of (18) and (19) performs an adaptive image smoothing and removes texture from an image.

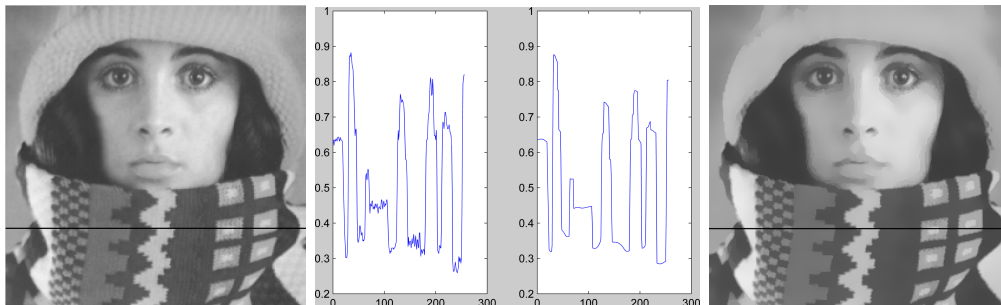


Figure 3: Demonstrating the power of nonlinear diffusion for image filtering. Left: original image “trui”. Right: after filtering with (18) and (19). Middle: a comparison of one-dimensional image slices of the original and filtered images.

In image processing, the system (18),(19) is typically solved by finite differences methods with explicit or implicit Euler schemes and several tens of iterations are usually required in order to achieve desired image filtering effects. For a number of applications including image segmentation and feature extraction, accurate estimation of the gradient directions in an image filtered by (18) and (19) is required. Unfortunately standard finite difference schemes have poor rotation-invariance properties. If such schemes are used repeatedly, the directional error is accumulated. See [28, 29] for examples of finite difference schemes with improved rotation invariance properties.

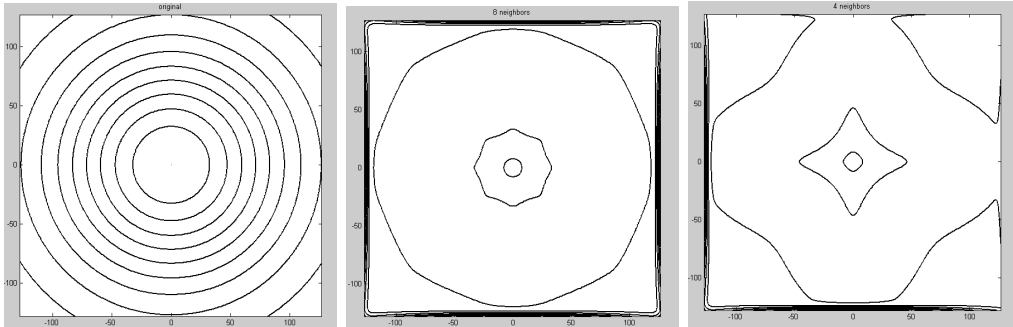


Figure 4: Left: the contour lines of Gaussian bump function (15) are perfect circles. Middle: contours of the Gaussian filtered using our implementation of nonlinear diffusion (18), (19). Right: contours of the Gaussian filtered using code from [20].

Our approach to numerical solving of (18), (19) combines the explicit Euler scheme with obvious generalizations of the optimal rotation-invariant 3×3 stencils derived in previous sections for gradient, Laplacian, and quasi Laplacian. To demonstrate advantages of our approach we apply our numerical implementation of (18), (19) to (15). Figure 4 shows level sets of (15) before and after applying nonlinear diffusion (18), (19). We also compare our implementation with that from [20], where five-point stencils are used for numerical solving (18) and (19).

We have chosen the system (18), (19) as a simple example and do believe that our approach can be employed for more accurate numerical solving of many other nonlinear PDEs used in image processing [1], computational fluid dynamics [6], and other disciplines.

Application to curvature estimation. So far we have considered function data defined on a regular grid. In the following examples, we deal with less organized data, namely with triangle meshes approximating smooth surfaces.

Reliable estimation of curvature characteristics of polygonal surfaces is very important for many computer graphics and geometric modeling applications. Starting from a seminal paper of Taubin [26] integral-based approaches are frequently used for curvature estimation purposes [15, 21, 16] (see also references therein). Our approach to curvature estimation is based on using discrete circular means of directional surface derivatives. Given a smooth

surface approximated by a dense triangle mesh, we employ such discrete circular means for estimating the mean curvature $H = (k_{\max} + k_{\min})/2$ and the so-called curviness [14] $R = \sqrt{(k_{\max}^2 + k_{\min}^2)}/2$, where k_{\max} and k_{\min} stand for the principal curvatures. (While curviness R is not a classical curvature measure, it is widely used in numerous applications including protein interaction analysis [5], heart physiology [30], and human visual perception [27].)

Let \mathbf{n} be a surface orientation normal. Denote by \mathbf{t}_{\max} and \mathbf{t}_{\min} the principal directions corresponding to the principal curvatures k_{\max} and k_{\min} , respectively. For a point P on the surface, consider a unit tangent vector $\mathbf{t}(\varphi)$, which makes angle φ with \mathbf{t}_{\max} , and the corresponding directional curvature $k(\varphi)$. Similar to (1) and (2) we have

$$H \equiv \frac{1}{2} (k_{\max} + k_{\min}) = \frac{1}{2\pi} \int_0^{2\pi} k(\varphi) d\varphi \quad (20)$$

and

$$R^2 \equiv \frac{1}{2} (k_{\max}^2 + k_{\min}^2) = \frac{1}{2\pi} \int_0^{2\pi} \left(\frac{\partial \mathbf{n}}{\partial \mathbf{t}(\varphi)} \right)^2 d\varphi, \quad (21)$$

respectively. Here (20) immediately follows from Euler's formula

$$k(\varphi) = k_{\max} \cos^2 \varphi + k_{\min} \sin^2 \varphi$$

and (21) is obtained from a similar representation

$$\left(\frac{\partial \mathbf{n}}{\partial \mathbf{t}(\varphi)} \right)^2 = k_{\max}^2 \cos^2 \varphi + k_{\min}^2 \sin^2 \varphi,$$

which, in its turn, can be easily derived from Rodrigues' formulas

$$\frac{\partial \mathbf{n}}{\partial \mathbf{t}_{\max}} = -k_{\max} \mathbf{t}_{\max}, \quad \frac{\partial \mathbf{n}}{\partial \mathbf{t}_{\min}} = -k_{\min} \mathbf{t}_{\min}.$$

Similar to (6) and (7), let us consider discrete counterparts of (20) and (21)

$$H = \sum w_j k(\varphi_j) \quad \text{and} \quad R^2 = \sum w_j \left(\frac{\partial \mathbf{n}}{\partial \mathbf{t}(\varphi_j)} \right)^2, \quad (22)$$

where weights $\{w_j\}$ satisfy (5) and are normalized. For the sake of simplicity, we use the set of weights (10) proposed in [15].

Consider now a triangle mesh approximating the surface and assume that each mesh vertex P is equipped with a unit normal $\mathbf{n}(P)$ which delivers a fairly good approximation of the corresponding surface normal. Given a mesh vertex P and its 1-ring neighboring vertices $\{Q_j\}$, as seen in the left image of Figure 5, simple approximations of tangential vectors at P and the corresponding directional curvature $k(\varphi_j)$ and directional derivative of \mathbf{n} are given by

$$\mathbf{t}_j \approx \frac{P\vec{Q}_j}{\|P - Q_j\|}, \quad k(\varphi_j) \approx \frac{2P\vec{Q}_j \cdot \mathbf{n}}{\|P - Q_j\|^2}, \quad \frac{\partial \mathbf{n}}{\partial \mathbf{t}_j} \approx \frac{\mathbf{n}(Q_j) - \mathbf{n}(P)}{\|Q_j - P\|}, \quad (23)$$

respectively. See the right image of Figure 5 for a geometric explanation of the directional curvature approximation. Finally, (22) and (23) provide us with discrete approximations of the mean curvatures H and curvedness R .

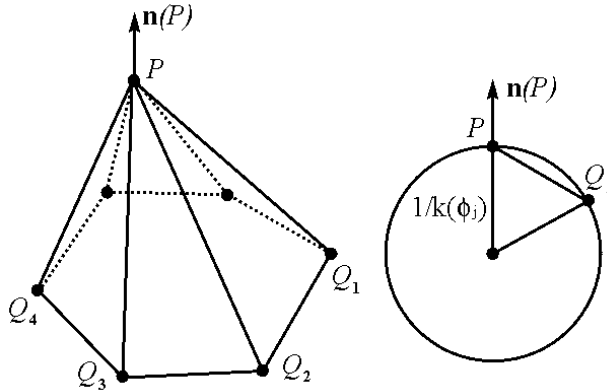


Figure 5: Left: a mesh vertex P and its 1-ring neighboring vertices $\{Q_j\}$. Right: a geometric explanation of the directional curvature approximation in (23).

Figure 6 presents color encodings for the mean curvature H and curvedness R detected on a geometrical model with many small-scale details.

A visual comparison of (22) and (23) with the curvature estimation methods developed in [26] and [21] indicates that our approach is less robust to noise but better reflects small-scale surface details.



Figure 6: Color encodings for the mean curvature (left) and curvedness (right) detected on Gargoyle model (center).

References

- [1] G. Aubert and P. Kornprobst. *Mathematical Problems in Image Processing*. Springer, 2nd edition, 2006.
- [2] Ei. Bannai and Et. Bannai. A survey on spherical designs and algebraic combinatorics on spheres. *European Journal of Combinatorics*, 30(6):1392–1425, 2009.
- [3] W. G. Bickley. Finite difference formulae for the square lattice. *Quart. J. Mech. Appl. Math.*, 1:35–42, 1948.
- [4] G. Birkhoff and R. E. Lynch. *Numerical Solution of Elliptic Problems*. SIAM, 1984.
- [5] J. R. Bradford and D. R. Westhead. Improved prediction of protein-protein binding sites using a support vector machines approach. *Bioinformatics*, 21(8):1487–1494, 2005.
- [6] S. Childress. Fast dynamo theory. In *Topological aspects of the dynamics of fluids*, pages 111–147, Dordrecht, 1992. Kluwer Academic Publishers.
- [7] P. Delsarte, J. M. Goethals, and J. J. Seidel. Spherical codes and designs. *Geometriae Dedicata*, 6:363–388, 1977.

- [8] A. Friedman and W. Littman. Functions satisfying the mean value property. *Transactions of the American Mathematical Society*, 102(1):167–180, 1962.
- [9] R. C. Gonzalez and R. E. Woods. *Digital Image Processing*. Pearson Prentice Hall, 3rd edition, 2008.
- [10] J. Harris. *Algebraic Geometry: A First Course*. Springer, 1992.
- [11] Y. Hong. On spherical t -designs in r^2 . *European Journal of Combinatorics*, 3:255–258, 1982.
- [12] Behz. Kamgar-Parsi, Behr. Kamgar-Parsi, and A. Rosenfeld. Optimally isotropic Laplacian operator. *IEEE Transactions on Image Processing*, 8(10):1467–1472, 1999.
- [13] L. V. Kantorovich and V. I. Krylov. *Approximate Methods of Higher Analysis*. Noordhoff-Interscience, 1956.
- [14] J. J. Koenderink and A. J. Van Doorn. Surface shape and curvature scales. *Image and Vision Computing*, 10:557–565, 1992.
- [15] T. Langer, A. Belyaev, and H.-P. Seidel. Exact and interpolatory quadratures for curvature tensor estimation. *Computer Aided Geometric Design*, 24(8-9):443–463, 2007.
- [16] Q. Mérigot, M. Ovsjanikov, and L. Guibas. Robust Voronoi-based curvature and feature estimation. In *Proc. of SIAM/ACM Joint Conference on Geometric and Physical Modeling*, pages 1–12, 2009.
- [17] F. Natterer. *The Mathematics of Computerized Tomography*. SIAM, 2001.
- [18] M. Patra and M. Karttunen. Stencils with isotropic discretisation error for differential operators. *Numerical Methods for Partial Differential Equations*, 22(4):936–953, 2005.
- [19] P. Perona and J. Malik. Scale-space and edge detection using anisotropic diffusion. *IEEE Transactions on Pattern Analysis and Machine Intelligence*, 12(7):629–639, 1990.

- [20] P. Perona, T. Shiota, and J. Malik. *Anisotropic Diffusion*, pages 73–92. Kluwer Academic Press, 1994.
- [21] H. Pottmann, J. Wallner, Q. Huang, and Y.-L. Yang. Integral invariants for robust geometry processing. *Computer Aided Geometric Design*, 26:37–60, 2009.
- [22] W. K. Pratt. *Digital Image Processing*. John Wiley & Sons, 3rd edition, 2001.
- [23] R. Schneider. *Convex Bodies: The Brunn-Minkowski Theory*. Cambridge University Press, 1993.
- [24] P. D. Seymour and T. Zaslavsky. Averaging sets: A generalization of mean values and spherical designs. *Advances in Math.*, 52:213224, 1984.
- [25] A. H. Stroud. *Approximate Calculation of Multiple Integrals*. Prentice-Hall, 1971.
- [26] G. Taubin. Estimating the tensor of curvature of a surface from a polyhedral approximation. In *Proc. ICCV'95*, pages 902–907, 1995.
- [27] R. Valenti, N. Sebe, and T. Gevers. Image saliency by isocentric curvedness and color. In *IEEE International Conference on Computer Vision*, 2009.
- [28] J. Weickert. Anisotropic diffusion filters for image processing based quality control. In *Proc. Seventh European Conf. on Mathematics in Industry*, pages 355–362. Teubner-Verlag, 1994.
- [29] J. Weickert and H. Schar. A scheme for coherence-enhancing diffusion filtering with optimized rotation invariance. *Journal of Visual Communication and Image Representation*, 13:103–118, 2002.
- [30] L. Zhong, Y. Su, S.-Y. Yeo, R.-S. Tan, D. N. Ghista, and G. Kassab. Left ventricular regional wall curvedness and wall stress in patients with ischemic dilated cardiomyopathy. *American Journal of Physiology - Heart and Circulatory Physiology*, 296:H573–H584, 2009.